Available online at www.elixirpublishers.com (Elixir International Journal)

Computational Physics

Elixir Computational Physics 102 (2017) 44325-44336

ISSN: 2229-712X

Isolation Spectroscopic Characterization of 3-Methyl-2-Nitroanisole by Density Functional Method

K.Parivathini[1], S.Manimaran[1], K.Sambathkumar[2,*], K.Settu[2] and A. Claude[2]

[1]Department of Physics,Thanthai Hans Rover College, Perambalur.

[2]Department of Physics, A.A.Govt.Arts College, TamilNadu, India.

ARTICLE INFO

Article history:

Received: 2 December 2016;

Received in revised form: 3 January 2017;

Accepted: 9 January 2017;

Keywords

FTIR,
FT-Raman,
MNA,
HOMO-LUMO,
NBO,
NMR.

ABSTRACT

A combined experimental and theoretical studies were conducted on the molecular structure and vibrational, spectra of 3-methyl-2-nitro anisole (MNA). The FT-IR and FT-Raman spectra of (MNA) were recorded in the solid phase. The molecular geometry and vibrational frequencies of MNA in the ground state have been calculated by using the ab-initio HF (Hartree-Fock) and density functional methods (B3LYP) invoking 6-31+G (d,p) basis set. The optimized geometric bond lengths and bond angles obtained by HF method shows best agreement with the experimental values. Comparison of the observed fundamental vibrational frequencies of MNA with calculated results by HF and density functional methods indicates that B3LYP is superior to the scaled HF approach for molecular vibrational problems. The difference between the observed and scaled wave number values of most of the fundamental is very small. The thermodynamic functions and atomic change of the title compound was also performed at HF/B3LYP/6-31+G(d,p) level of theories. A detailed interpretation of the NBO, NMR spectra of MNA was also reported. The thermodynamic function of the title compound was also performed at HF/6-31+G (d,p) and B3LYP/6-31+G (d,p) level of theories. Natural bond orbital analysis has been carried out to explain the change transfer or delocalization of change due to the intra-molecular interactions. Energy of the highest occupied molecular (HOMO) orbital and lowest unoccupied (LUMO) molecular orbital have been predicted.

1. Introduction

Anisole is a crystalline powder that is soluble in ether and alcohol insoluble in water; boiling point 155°C. Anisole is more electron rich than benzene because of the resonance effect of the methoxy group[1]. Anisole reacts with electrophilic aromatic substitution reaction quickly than benzene. Anisole has the two effects, i.e. back-donation and conjugation, can be competitive and their relative weight determining the electronic properties of the molecule can be conformation independent[2]. Anisole is used in perfumery, chemical syntheses and an insect pheromone. Particularly anisole is a bio-agent and it is mainly used to synthesize amino anisole, dyes and medicine. The application of anisole as a detector for middle infrared interferometry [3] has been confirmed. Since the anisole absorbs IR radiation heat it is possible to estimate the IR intensity distribution on the anisole from the diffraction pattern made by visible larger light that is transmitted through it. It is used to measure the mono phenolase activity of polyphenol oxidize from fruits and vegetables [4]. Other antioxidants for food are phosphoric acid, citric acid, gallic acid, ascorbic acid and their esters which form complexes with the pro-oxidative metal traces. Antimicrobial process is also important in preserving foods. MNA are used as an antioxidant in plastics, elastomers and petroleum (lubes, greases and waxes), practically bigger market size than food field. MNA is used as a stabilizer to inhibit the auto-polymerization of organic peroxides. More recently, the experimental vibrational spectra of p-nitroanisole, 2-nitroanisole, thioanisole, and 3-nitroanisole [5] have been investigated in comparison with DFT/B3LYP level calculations.In the case of IR laser interferometry, interference fringe patterns that are created by the IR laser on the anisole are observed as the refractive index distribution; hence the anisole functions as a phase grating for visible light. It is, therefore, conceivable to estimate the IR intensity distribution on the anisole by analyzing the diffraction pattern made by a visible laser, which is transmitted through the anisole. Also, since a two dimensional device using the anisole does not require matrix structure, it is expected that the measurement system must have high spatial resolution, equivalent to that of existing IR cameras. Owing to these applications and the reliable properties of anisole, a complete vibrational study on 3-methyl-2-nitroanisole (MNA) has been undertaken. The vibrational analyses of MNA using the SQM force field method based on DFT calculation have been presented. The calculated infrared and Raman spectra of MNA are also simulated utilizing the computed dipole derivatives for IR intensities and polarizability derivatives for Raman activities.

2. Experimental Analysis

The chemicals required were obtained from Sigma Aldrich chemical suppliers and are of analar grade. FTIR spectra (KBr pellets) were recorded on 8101 Schimadzu FTIR spectrophotometer recorded in the region 4000 - 400 cm^{-1}. FT-Raman spectra have been recorded in the region 3500 - 50 cm^{-1}on a Perkin-Elmer spectrometer.

Tele: 09994188861
E-mail address: sa75kumar@yahoo.co.in

3. Computational Methodology

The entire calculations are performed at Hartree-Fock (HF) and density functional (DFT) levels using GAUSSIAN 09W [6] program package, invoking gradient geometry optimization [7]. Initial geometry generated from the standard geometrical parameters was minimized without any constraint on the potential energy surface at HF level adopting the standard 6-311++G(d,p) basis set. This geometry was then re-optimized again at DFT level employing the Becke 3LYP keyword, which invokes Becke's three-parameter hybrid method [8] using the correlation function of Lee *et al.* [9]; implemented with the same basis set. The optimized structural parameters are used for the vibrational frequency calculations at DFT level to characterize all the stationary points as minima. The multiple scaling of the force constants are performed according to SQM procedure [10,11] using selective scaling in the natural internal coordinate representation [12,13]. The transformation of force field; subsequent normal coordinate analysis and calculation of the TED are done on a PC with MOLVIB program (version V7.0 – G77) written by Sundius [14-16]. By the use of GAUSSVIEW molecular visualization program [17] along with available related molecules; the vibrational frequency assignments are made by their TED with a high degree of confidence. The TED elements provide a measure of each internal co-ordinate's contributions to the normal coordinate.

3.1. Prediction of Raman intensities

The Raman activities (S_i) calculated with the GAUSSIAN 09W program are subsequently converted to relative Raman intensities (I_i) using the following relationship derived from the basic theory of Raman scattering [18-20]

$$I_i = \frac{f\left(\nu_o - \nu_i\right)^4 S_i}{\nu_i\left[1 - \exp\left(-hc\nu_i/kT\right)\right]} \quad \text{... (1)}$$

where ν_0 is the exciting frequency in cm^{-1}, ν_i the vibrational wave number of the ith normal mode, *h*, *c* and *k* are the fundamental constants and *f* is a suitably chosen common normalisation factor for all the peak intensities.

4. Results and Discussion

4.1. Molecular geometry

The molecular structure of MNA belongs to C_1 point group symmetry. For C_1 symmetry there would not be any relevant distribution. The molecule consists of 21 atoms and expected to have 57 normal modes of vibrations of the same a species under C_1 symmetry. These modes are found to be IR and Raman active suggesting that the molecule possesses a non-centrosymmetric structure, which recommends the MNA for non-linear optical applications. The optimized molecular structure of MNA is shown in Fig. 1, respectively.

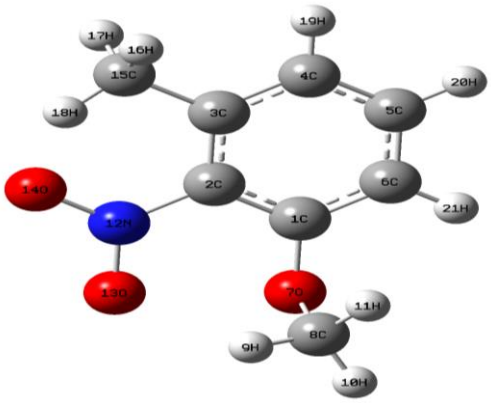

Fig 1. Molecular structure of 3-methyl-2-nitro anisole.

4.2. PES scan studies

The potential energy surface (PES) scan with the B3LYP/6-311++G(d,p) level of theoretical approximations was performed for MNA is shown in Fig. 2, respectively. The dihedral angle C1–C2–N12–O14 for MNA is also relevant coordinate for conformational flexibility within the molecule. During the calculation, all the geometrical parameters are simultaneously relaxed while the C1–C2–N12–O14 torsional angle are varied in steps of 10°, 20°, 30°,..., 360°. For this rotation minimum energy curves have been obtained at 0°, 110° and 250° as shown in Figs. 3 and 4 clearly demonstrates that 0° corresponds to the global minimum energy is –590.54807307 Hartrees for MNA, respectively and the minimum energy for the rotation at 110° and 250° are –590.54780773, –590.54784943 Hartrees for MNA, respectively. The maximum energy is obtained at 180° for both the molecules.

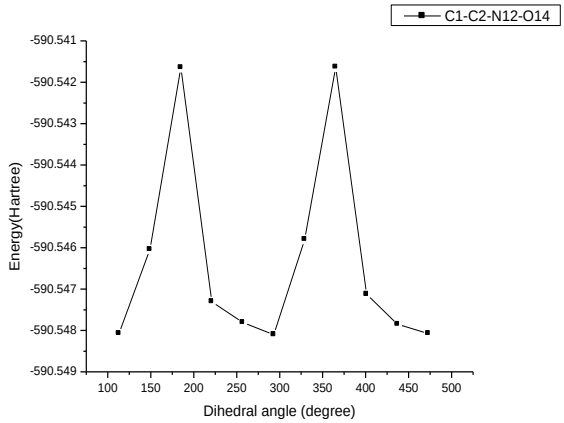

Fig 2. PES scan of 3-methyl-2-nitro anisole.

4.3. Structural properties

The optimization geometrical parameters of MNA obtained by the *ab initio* HF and DFT/B3LYP methods with 6-311++G(d,p) as basis set are listed in Table 1. The computed bond length and bond angles are compared with X-ray diffraction data of similar compound [21]. From Table 1, it can be seen that there are some deviations in the computed geometrical parameters from those reported in the single crystal XRD data, and these differences are probably due to the intermolecular interactions in the crystalline state. Comparing bond angles and bond lengths of B3LYP method with HF method, various bond lengths are found to be almost same at HF/6-311++G(d,p) and B3LYP/6-311++G(d,p) levels. However, the B3LYP/6-311++G(d,p) level of theory, in general slightly over estimates bond lengths but it yields bond angles in excellent agreement with the HF method. For the investigated molecule, the benzene ring appears a little distorted with larger C4–C5, C1–C2 bond length and shorter C1–C2, C4–C5 bond length and angles slightly out of the regular hexagonal structure for MNA. These distortions are explained in terms of the change in hybridisation affected by the substituent at the carbon site to which it is appended. The MNA of C–C bond lengths adjacent to the C3–O15, C8–O7 bonds are increases and the angles C2–C1–C6, C2-C3-C4, C1-C6-C5 are smaller than typical hexagonal angle of 120°. This is because of the effect of substitution of O–CH_3 groups attached to the C6 and C1 of the benzene ring for MNA. The variation in torsional angles C6–C1–O7–C8 = 77.01° (HF), –2.15° (B3LYP) is due to charge delocalization for MNA. The calculated geometric parameters can be used as foundation to calculate the other parameters for the molecule.

Table 1. Optimized geometrical parameters of 3-methyl-2-nitroanisole by using B3LYP/6-311+G(d,p) and B3LYP/ 6-311++G(d,p) methods and basis set calculations.

Bond Length	Value (Å)		Exp	Bond Angle	Value (°)		Exp	Dihedral Angle	Value (°)	
	HF/ 6-311++G(d,p)	B3LYP/ 6-11++G(d,p)			HF/ 6-311++G(d,p)	B3LYP/ 6-311++G(d,p)			HF/ 6-311++G(d,p)	B3LYP/ 6-311++ (d,p)
C1-C2	1.3862	1.4028		C2-C1-C6	118.5865	118.1802		C6-C1-C2-C3	-0.0735	-0.473
C1-C6	1.3866	1.3966		C2-C1-O7	119.7595	116.589		C6-C1-C2-N12	179.9527	179.2257
C1-O7	1.3485	1.3527		C6-C1-O7	121.5198	125.2154		O7-C1-C2-C3	-175.9267	178.1723
C2-C3	1.3903	1.3936		C1-C2-C3	123.3382	123.3088	117.82	O7-C1-C2-C12	4.0995	-2.1291
C2-N12	1.4641	1.4807	1.491	C1-C2-N12	117.5613	117.7382	118.6	C2-C1-C6-C5	1.0595	-0.3454
C3-C4	1.3892	1.3999		C3-C2-N12	119.1005	118.9523		C2-C1-C6-H21	-177.959	179.6272
C3-C15	1.511	1.508		C2-C3-C4	116.6463	117.0158		O7-C1-C6-C5	176.8364	-178.8625
C4-C5	1.3872	1.3898		C2-C3-C15	122.4958	121.8525		O7-C1-C6-H21	-2.1821	1.1101
C4-H19	1.0748	1.0835	1.090	C4-C3-C15	120.8559	121.13		C2-C1-O7-C8	-107.2579	179.3024
C5-C6	1.3829	1.3934		C3-C4-C5	121.0881	120.7999		C6-C1-O7-C8	77.0138	-2.1593
C5-H20	1.0753	1.084	1.090	C3-C4-H19	119.1763	119.0847		C1-C2-C3-C4	-1.0861	1.1012
C6-H21	1.0743	1.0811	1.091	C5-C4-H19	119.7346	120.1154		C1-C2-C3-C15	179.4303	-179.3608
O7-C8	1.4172	1.4246		C4-C5-C6	120.8808	121.2027		N12-C2-C3-C4	178.8874	-178.594
C8-H9	1.0823	1.0946	1.090	C4-C5-H20	119.5668	119.7141		N12-C2-C3-C15	-0.5962	0.944
C8-H10	1.0794	1.0879	1.090	C6-C5-H20	119.5492	119.0831		C1-C2-N12-O13	-177.2474	113.0626
C8-H11	1.0845	1.0944	1.090	C1-C6-C5	119.4417	119.483		C1-C2-N12-O14	63.9021	-68.2033
N12-O13	2.6681	1.224	1.227	C1-C6-H21	119.2362	120.5328		C3-C2-N12-O13	62.7776	-67.2252
N12-O14	1.1924	1.2205	1.228	C5-C6-H21	121.3146	119.9842		C3-C2-N12-O14	-116.0729	111.5089
C15-H16	2.7286	1.0904		C1-O7-C8	117.0894	118.9148	117.64	C2-C3-C4-C5	1.2815	-0.9304
C15-H17	1.0824	1.0934		O7-C8-H9	110.3512	111.2231	117.80	C2-C3-C4-H19	-179.0757	179.0448
C15-H18	1.0832	1.0926		O7-C8-H10	106.0602	105.5137	117.80	C15-C3-C4-C5	-179.2259	179.5281
				O7-C8-H11	110.7278	111.129	117.80	C15-C3-C4-H19	0.4169	-0.4968
				H9-C8-H10	109.8492	109.5129	124.31	C2-C3-C15-H16	166.7484	-170.8561
				H9-C8-H11	110.1785	109.8752		C2-C3-C15-H17	-73.1455	-50.6739
				H10-C9-H11	109.5918	109.4847		C2-C3-C15-H18	46.8301	68.859
				C2-N12-O13	112.7465	117.1751		C4-C3-C15-H16	-12.7139	8.6631
				C2-N12-O14	117.4204	117.4914		C4-C3-C15-H17	107.3922	128.8453

[a] For numbering of atoms refer Fig. 2. [a] Experimental values are taken from Ref. [21].

5. vibrational spectra

Detailed description of vibrational modes can be given by means of normal coordinate analysis. For this purpose, the full set of 71 standard internal coordinates (containing 14 redundancies) for MNA are presented in Table 2, respectively. From these, a non-redundant set of local symmetry coordinates are constructed by suitable linear combinations of internal coordinates following the recommendations of Fogarasi *et al.* and they are summarized in Table 3 for MNA, respectively. The detailed vibrational assignment of fundamental modes of MNA along with the calculated IR, Raman frequencies and normal mode descriptions (characterized by TED) are reported in Table 4. For visual comparison, the observed and calculated FTIR and FT-Raman spectra of MNA at HF and B3LYP levels using 6-311++G(d,p) basis set are shown in Figs. 3 - 4. The vibrational analysis obtained for MNA with the unscaled HF and B3LYP/6-311++G(d,p) force field are generally somewhat greater than the experimental values due to neglect of anharmonicity in real system. These discrepancies can be corrected either by computing anharmonic corrections explicitly or by introducing a scaled field or directly scaling the calculated wave numbers with proper factor [22]. A tentative assignment is often made on the basis of the unscaled frequencies by assuming the observed frequencies so that they are in the same order as the calculated ones. Then, for an easier comparison to the observed values, the calculated frequencies are scaled by the scale to less than 1, to minimize the overall deviation. The results indicate that the B3LYP calculations approximate the observed fundamental frequencies much better than the HF results. Inclusion of electron correlation in density functional theory to a certain extent makes the frequency values smaller in comparison with HF frequency. Also, it should be noted that the experimental results belong to solid phase and theoretical calculations belong to gaseous phase. A better agreement between the computed and experimental frequencies can be obtained by using different scale factors for different regions of vibrations. For that purpose, we have utilized different scaling factors for all fundamental modes except the torsional mode to obtain the scaled frequencies of the compound. The resultant scaled frequencies are also listed in Table 4.

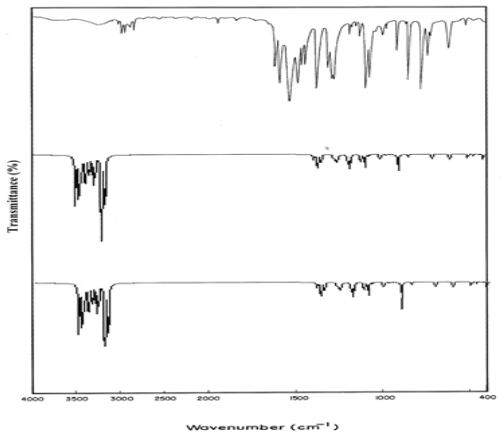

Fig 3. Comparison of observed and calculated infrared spectra of 3-methyl-2-nitro anisole.

(a) Observed
(b) HF/6-311++G(d,p)
(c) B3LYP/6-311++G(d,p)

Table 2. Definition of internal coordinates of 3-methyl-2-nitroanisole.

No. (i)	Symbol	Type	Definition[a]
Stretching			
1-3	r_i	CH	C4-H19, C5-H20, C6-H21
4-9	η_i	CH_3(methyl)	C8-H9, C8-H10, C8-H11, C15-H16, C15-H17,C15-H18
10-11	R_i	CO	C1-O7, C8-O7
12-18	q_i	CC	C1-C2, C2-C3, C3-C4, C4-C5, C5-C6, C6-C1, C3-C15
19	S_i	CN	C2-N12
20-21	X_i	NO	N12-O13, N12-O14
In-plane bending			
22-27	α_i	Ring	C1-C2-C3, C2-C3-C4, C3-C4-C5, C4-C5-C6, C5-C6-C1, C6-C1-C2
28-33	β_i	CCH	C1-C6-H21, C5-C6-H21, C6-C5-H20, C4-C5-H20, C5-C4-H19, C3-C4-H19
34-35	π_i	CCC	C2-C3-C15, C4-C3-C15
36-37	θ_i	CCO	C6-C1-O7, C2-C1-O7
38	θ_i	COC	C1-O7-C8
39-41	υ_i	CCH(methyl)	C3-C15-H16, C3-C15-H17, C3-C15-H18
42-44	β_i	HCH	H16-C15-H17, H17-C15-H18, H16-C15-H18
45-47	υ_i	OCH	O7-C8-H9, O7-C8-H10, O7-C8-H11
48-50	β_i	HCH	H9-C8-H10, H10-C8-H11, H9-C8-H11
51-52	$£_i$	CCN	C3-C2-N12, C1-C2-N12
53-54	ψ_i	CNO	C2-N12-O13, C2-N12-O14
55	ρ_i	O-N-O	O13-N12-O14
Out-of-plane bending			
56-58	δ_i	CH	H19-C5-C4-C3, H20-C5-C6-C4, H21-C6-C1-C5
59	ψ_i	OC	O7-C1-C2-C6
60	λ_i	OC	C8-O7-C1-(C6-C2)
61	δ_i	CC	C15-C3-C2-C4
62	χ_i	CN	N12-C2-C3-C1
Torsion			
63-68	τ_i	tRing	C1-C2-C3-C4, C2-C3-C4-C5, C3-C4-C5-C6, C4-C5-C6-C1, C5-C6-C1-C2, C6-C1-C2-C3
69	τ_i	tC-CH_3	(C2-C4)-C3-C15-(H16,H17,H18)
70	τ_i	tO-CH_3	C1-O7-C8-(H9,H10,H11)
71	τ_i	tC-NO_2	(C1-C2)-C2-N12-(O13,O14)

[a]For numbering of atoms refer Fig. 2.

C–H vibrations The hetero aromatic structure shows the presence of C–H stretching vibration in the region 3100 – 3000 cm^{-1} which is the characteristic region for the identification of such C–H stretching vibrations. These vibrations are not found to be affected due to the nature and position of the substituents. In the present investigation, the C–H vibrations are observed at 3101, 3082, 3030 cm^{-1} in FT-Raman spectrum for MNA and the corresponding force constant contribute to the TED for MNA. The C-H in-plane-bending vibrations usually occur in the region 1390 - 990 cm^{-1} and are very useful for characterization purposes. The C–H out-of-plane bending vibrations occur in the region 900 - 675 cm^{-1} and these bands are highly informative [22]. Accordingly, the 998, 976 cm^{-1} in the FTIR spectrum and 1001 cm^{-1} in Raman spectrum for MNA have been assigned to, C–H in-plane-bending vibrations. The C–H out-of-plane mode is observed at 776, 745 cm^{-1} in the FTIR and at 752 cm^{-1} in Raman spectrum for MNA.

The observed C–H out-of-plane bending modes show consistent agreement with the computed B3LYP and HF results. *C–C vibrations* The C–C hetero aromatic stretching vibrations generally occur in the region 1650 - 1400 cm^{-1} [22]. With heavy substituents, the bonds tend to shift to somewhat lower wavenumbers and greater the number of substituents on the ring, broader the absorption regions. As predicted in the earlier references, in the present investigation, the C–C stretching vibrations for MNA, the FTIR peaks observed at 1586, 1522, 1374 and 1310 cm^{-1} and in FT-

Table 3. Definition of local symmetry coordinates of 3-methyl-2-nitroanisole.

No	Type	Definition[a]
1-3	CH	r_1, r_2, r_3
4,5	CH_3ss	$\eta_4 + \eta_5 + \eta_6 / \sqrt{3}$, $\eta_7 + \eta_8 + \eta_9 / \sqrt{3}$
6,7	CH_3ips	$2\eta_4 + \eta_5 + \eta_6 / \sqrt{6}$, $2\eta_7 + \eta_8 + \eta_9 / \sqrt{6}$
8,9	CH_3ops	$\eta_5 - \eta_6 / \sqrt{6}$, $\eta_8 - \eta_9 / \sqrt{6}$
10,11	CO	R_{10}, R_{11}
12-18	CC	$q_{12}, q_{13}, q_{14}, q_{15}, q_{16}, q_{17}, q_{18}$
19	CN	S_{20}
20	NO_2ss	$X_{20} - X_{21}/ \sqrt{2}$
21	NO_2ass	$X_{20} + X_{21}/ \sqrt{2}$
22	Rtrigd	$(\alpha_{22} - \alpha_{23} + \alpha_{24} - \alpha_{25} + \alpha_{26} - \alpha_{27}) / \sqrt{6}$
23	Rsymd	$(-\alpha_{22} - \alpha_{23} + 2\alpha_{24} - \alpha_{25} - \alpha_{26} + 2\alpha_{27}) / \sqrt{12}$
24	Rasymd	$(\alpha_{22} - \alpha_{23} + \alpha_{25} - \alpha_{26}) / \sqrt{2}$
25-27	bCH	$\beta_{28} - \beta_{29} / \sqrt{2}$, $\beta_{30} - \beta_{31} / \sqrt{2}$, $\beta_{32} - \beta_{33} / \sqrt{2}$
28	bCC	$\pi_{34} - \pi_{35}/ \sqrt{2}$
29	bCO	$\theta_{36} - \theta_{37}/ \sqrt{2}$
30	bOC	θ_{38}
31-32	CH_3 sb	$(-\upsilon_{39} - \upsilon_{40} - \upsilon_{41} + \beta_{42} + \beta_{43} + \beta_{44})/ \sqrt{2}$, $(-\upsilon_{45} - \upsilon_{46} - \upsilon_{47} + \beta_{48} + \beta_{49} + \beta_{50})/ \sqrt{2}$
33-34	CH_3 ipb	$(2\beta_{44} - \beta_{43} - \beta_{42})/ \sqrt{6}$, $(2 \beta_{50} - \beta_{49} - \beta_{48})/ \sqrt{6}$
35-36	CH_3 opb	$(\beta_{42} - \beta_{43} / \sqrt{6}$, $(\beta_{48} - \beta_{49} / \sqrt{6}$
37-38	CH_3 ipr	$(2\upsilon_{39} + \upsilon_{40} - \upsilon_{41})/ \sqrt{6}$, $(2\upsilon_{45} + \upsilon_{46} - \upsilon_{47})/ \sqrt{6}$
39-40	CH_3 opr	$(\upsilon_{40} - \upsilon_{41})/ \sqrt{2}$, $(\upsilon_{46} - \upsilon_{47})/ \sqrt{2}$
41	£CN	$(£_{51} - £_{52})/ \sqrt{2}$
42	NO_2rock	$\psi_{53} - \psi_{54}/ \sqrt{2}$
43	NO_2twist	$\psi_{53} - \psi_{54}/ \sqrt{2}$
44	NO_2sciss	$2\rho_{55} - \psi_{54} - \psi_{53}/ \sqrt{2}$
45-47	δCH	$\delta_{56}, \delta_{57}, \delta_{58}$
48	ψCO	ψ_{59}
49	λOC	λ_{60}
50	λCC	δ_{61}
51	χCN	χ_{62}
52	tRtrigd	$(\tau_{63} - \tau_{64} + \tau_{65} - \tau_{66} + \tau_{67} - \tau_{68}) / \sqrt{6}$
53	tRsymd	$(\tau_{63} - \tau_{65} + \tau_{67} - \tau_{68}) / \sqrt{2}$
54	tRasymd	$(-\tau_{63} + 2\tau_{64} - \tau_{65} - \tau_{66} + 2\tau_{67} - \tau_{68}) / \sqrt{12}$
55	tCH_3	τ_{69}
56	$tOCH_3$	τ_{70}
57	NO_2wag	τ_{71}

[a] The internal coordinates used here are defined in Table 4.

Raman the peaks are observed at 1559, 1538, 1489, 1374 and 1311 cm^{-1} are assigned for C–C stretching vibrations are confirmed by their TED values. Most of the ring vibrational modes are affected by the substitutions in the hetero aromatic ring of MNA. The bands observed at 728 cm^{-1} in the FTIR for MNA have been designated to ring in-plane bending modes by careful consideration of their quantitative descriptions. The ring out-of-plane bending modes of MNA are also listed in Table 4 respectively.

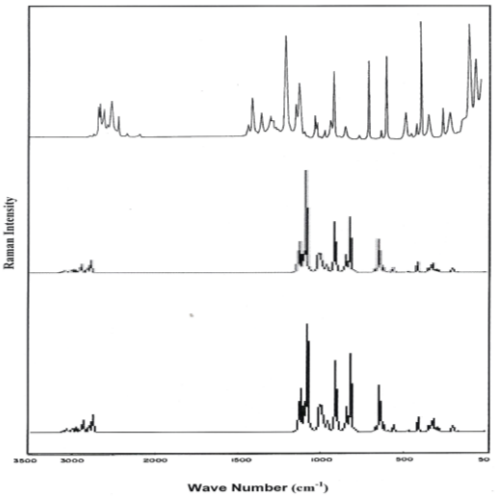

Fig 4.Comparison of observed and calculated Raman spectra of 3-methyl-2-nitro anisole.

(a) Observed
(b) HF/6-311++G(d,p)
(c) B3LYP/6-311++G(d,p)

C–O vibrations The interaction of the carbonyl group with a hydrogen donor group does not produce drastic and characteristic changes in the frequency of the C=O stretch as does by O–H stretch. A great deal of structural information can be derived from the exact position of the carbonyl stretching absorption peak. Susi and Ard [22] identified the C=O stretching mode at 1645 and 1614 cm^{-1}. On referring to the above findings and on the basis of the results of the normal coordinate analysis, the present investigation, the C–O

stretching vibrations have been found at 1189, 1178 cm^{-1} in IR for MNA are assigned for C–O stretching vibrations are confirmed by their TED values. The C–O in-plane and out-of-plane bending vibrations level also have been identified and presented in Table 4 respectively for MNA.

CH_3 group vibrations The investigated molecule under consideration possesses CH_3 groups in third position of MNA in the ring. For the assignments of CH_3 group frequencies one can expected that nine fundamentals can be associated to each CH_3 group, namely three stretching, three bending, two rocking modes and a single torsional mode describe the motion of methyl group. The CH_3 symmetric stretching frequency is identified at 2983 cm^{-1} in the FTIR and 2951 cm^{-1} in the FT-Raman spectrum for MNA. The CH_3 in-plane stretching vibrations are identified at 2929 cm^{-1} in FT-Raman spectrum and 2940 cm^{-1} in the FTIR spectrum for MNA. The CH_3 symmetric bending and CH_3 in-plane bending frequencies are attributed at 1274 cm^{-1} and 1462, 1441 cm^{-1} in the FTIR spectrum and 1263 cm^{-1} FT-Raman spectrum for MNA. These assignments are supported by literature [22]. The in-plane rocking and out-of-plane rocking modes of CH_3 group are found at 916 cm^{-1} and 1154 cm^{-1} in the FTIR spectrum and 883, 1164 cm^{-}in the FT-Raman spectrum for MNA. The bands obtained at 2894, 2846 cm^{-1} and 1130 cm^{-1} in the FTIR and 2847 cm^{-1} and 1142 cm^{-1} FT-Raman spectrum for MNA assigned to CH_3 out-of-plane stretching and CH_3 out-of-plane bending modes, respectively. The assignment of the bands at 215, 176 cm^{-1} FT-Raman spectrum for MNA attributed to methyl twisting mode.

NO_2 vibrations There are six normal modes due to an NO_2 group namely asymmetric NO_2 stretching, symmetric NO_2 stretching, NO_2 rocking, NO_2 wagging and NO_2 torsion. The NO_2 asymmetric stretching vibration band range is 1625 - 1540 cm^{-1} and that of symmetric stretching vibration is 1400 - 1360 cm^{-1} [22]. In the present investigation, the NO_2 asymmetric stretching vibrations for both IR and Raman spectrum is observed at 1613 cm^{-1}. The symmetric stretching vibration is observed at 1285 cm^{-1} in FTIR spectrum for MNA. The NO_2 scissoring vibration is observed at 851 cm^{-1} in IR spectrum. The deformation vibrations of NO_2 group (rocking, wagging and twisting) contribute to several normal modes in the low frequency region. These bands are also found well within the characteristic region and are summarized in Table 4.

5.1. Molecular properties

The thermodynamic parameters namely heat capacity, entropy, rotational constants, dipole moments, vibrational and zero-point vibrational energies of the compound have also been computed at *ab initio* HF and DFT/B3LYP levels using 6-311++G(d,p) as basis set and are presented in Table 5 for MNA, respectively. The difference in the values calculated by both the methods is marginal. The variation in the ZPVE seems to be insignificant. The ZPVE is much lower by the DFT/B3LYP method than by the HF method. The total energy and the change in the total entropy of the molecule at room temperature are also presented. Dipole moment reflects the molecular charge distribution and is given as a vector in three dimensions. Therefore, it can be used as descriptor to depict the charge movement across the molecule. Direction of the dipole moment vector in a molecule depends on the centers of positive and negative charges. Dipole moments are strictly determined for neutral molecules. For charged systems, its value depends on the choice of origin and molecular orientation. As a result of HF and DFT (B3LYP) calculations, the highest dipole moment is observed for B3LYP/6-311++G(d,p) level whereas the lowest one is observed for HF/6-311++G(d,p) level in the molecule.

The total dipole moment of MNA determined by HF and B3LYP level using 6-311++G(d,p) basis set is 0.9606, 1.2182 Debye, respectively.

6. Prediction of First Hyperpolarizability

The first hyperpolarizability (β_0) of this novel molecular system and the related properties (β_0, α_0) of MNA are calculated using the B3LYP/ 6-311++G(d,p) basis set, based on the finite field approach. In the presence of an applied electric field, the energy of a system is a function of the electric field. The first hyperpolarizability is a third-rank tensor that can be described by a $3 \times 3 \times 3$ matrix[23]. The 27 components of the 3D matrix can be reduced to 10 components due to the Kleinman symmetry. It can be given in the lower tetrahedral. The components of β are defined as the coefficients in the Taylor series expansion of the energy in the external electric field.

When the external electric field is weak and homogenous, this expansion becomes:

$$E = E_0 - \mu_\alpha F_\alpha - \frac{1}{2}\alpha_{\alpha\beta}F_\alpha F_\beta - \frac{1}{6}\beta_\alpha\beta_\gamma F_\alpha F_\beta F_\gamma + \ldots$$

Table 4. The observed (FTIR and FT-Raman) and calculated (unscaled and scaled) fundamental harmonic frequencies (cm^{-1}), force constant (mdyn A^{-1}), infrared - intensity (km/mol), Raman activity (Å amu^{-1}) and probable assignments of 3-methyl-2-nitroanisole are analysed based on SQM force field calculation using HF/6-311++G(d,p) and B3LYP/6-311++G(d,p) method and basis set calculations.

Observed frequencies		HF/6-311++G(d,p)					B3LYP/6-311++G(d,p)					Assignments (TED %)
FTIR	FT-Raman	Unscaled	Scaled	Force Const	IR intensity	Raman activity	Unscaled	Scaled	Force Const	IR intensity	Raman activity	
-	3101w	3382	3221	7.3969	6.8601	165.695	3213	3105	6.6446	3.4982	118.02	υCH(99)
-	3082w	3370	3258	7.3202	14.0719	14.0719	3212	3088	6.5533	12.3767	154.92	υCH(98)
-	3030vw	3353	3222	7.2153	3.2637	57.4249	3192	3035	6.4468	3.1175	60.322	υCH(97)
2983vw	-	3321	3196	7.1914	27.3335	100.915	3146	2987	6.4142	12.9628	102.83	CH3 ss(90), CH3ips(10)
-	2951w	3284	3129	7.0208	15.8950	58.8190	3129	2954	6.3187	12.8697	56.891	CH3ss(87), CH3ips(13)
2940vw	-	3281	3100	7.0027	26.9387	42.8831	3094	2946	6.0241	6.3240	62.982	CH3ips(79), CH3 ss(20)
-	2929vw	3270	3087	6.9478	12.1930	59.1378	3077	2935	6.1767	29.5562	56.985	CH3ips(71), CH3 ss(26)
2894vw	-	3203	3058	6.2685	16.9173	173.631	3038	2899	5.6411	12.8974	204.01	CH3ops(74), υCC(24)
2846vw	2847w	3201	3074	6.2460	58.0375	84.1631	3054	2858	5.5360	49.9870	158.51	CH3ops(79), υCC(20)
1613ms	1613w	1827	1766	22.796	624.865	3.4224	1696	1619	12.2869	92.9804	10.296	NO2ass(89), CH3ops(11)
1586ms	-	1789	1682	14.563	103.540	16.6865	1669	1597	8.4660	71.0762	32.102	υCC(63), CH3ops(32)
-	1559vw	1780	1595	11.140	67.6607	18.7550	1595	1565	18.4206	275.226	12.282	υCC(88), NO2ass(12)
-	1538w	1756	1575	18.392	107.991	20.7632	1565	1544	2.2006	69.8124	7.5901	υCC(77), CH3ipb(21)
1522vs	-	1699	1554	3.3958	82.3702	3.0327	1556	1528	1.8615	35.3634	4.9048	υCC(73), CH3ipb(22)
-	1489vs	1671	1543	1.6777	9.7713	7.4470	1510	1498	1.6404	14.1779	1.0648	υCC(85)
1462s	-	1666	1523	2.2926	16.6797	3.9792	1501	1468	1.3735	8.5311	12.606	CH3ipb(80), υCC(19)
1441s	-	1650	1593	1.6288	8.4194	11.2090	1545	1446	1.5087	24.5830	5.8904	CH3ipb(82), υCC(18)
1374ms	1374w	1634	1588	1.8083	17.7256	6.8157	1497	1385	1.6906	6.7976	2.9291	υCC(79), NO2ss(20)
1310vs	1311ms	1626	1578	1.9015	11.2427	4.0213	1461	1324	2.1681	22.2932	1.4018	υCC(73), CH3sb(19)
1285s	-	1612	1450	2.5002	16.4548	3.3615	1420	1288	1.4705	1.4454	14.042	NO2ss(75), υCC(25)
1274vw	-	1552	1437	1.7368	0.6752	6.8007	1407	1276	14.6833	143.327	22.193	CH3sb(64), υCN(30)
-	1263w	1429	1407	4.0781	141.329	19.3044	1339	1266	5.7839	60.3669	14.314	CH3sb(65), υCO(32)
1255s	-	1388	1386	1.9649	2.7693	2.0602	1308	1258	3.7019	150.593	19.388	υCN(66), CH3sb(36)
1189vw	-	1324	1297	1.6677	1.5622	3.0395	1278	1193	1.8984	2.9039	3.1854	υCO(72), CH3opr(22)
1178vw	-	1306	1260	1.4878	4.6140	1.1436	1208	1182	1.1473	1.2083	9.4959	υCO(78), CH3opr(21)
-	1164vs	1279	1216	1.2068	2.5699	3.0848	1196	1166	1.0774	0.0425	1.0606	CH3opr(74), υCO(20)
1154vs	-	1255	1201	2.9981	10.5563	1.5368	1168	1157	1.0201	0.9366	2.2797	CH3opr(73), CH3opb(22)
-	1142w	1232	1194	2.0080	5.0160	6.8829	1147	1145	1.6734	7.2738	1.0146	CH3opb(77), Rasym(26)
1130vs	-	1188	1168	3.1425	127.927	8.6351	1118	1135	3.0546	97.978	1.6004	CH3opb(73), Rsymd(21)
1091ms	-	1166	1144	1.5915	5.9780	5.1572	1102	1093	2.5356	12.444	24.322	Rasym(72), Rtrigd(22)
1070ms	-	1162	1111	1.6635	19.2732	6.1602	1099	1077	1.0122	2.1580	0.6462	Rsymd(71), bCH(29)

-	1024vs	1116	1076	1.0191	3.4024	0.8975	1066	1029	1.1639	17.693	5.6861	Rtrigd(70), bCH(28)
-	1001w	1106	1069	1.4157	12.3866	10.5245	1045	1009	0.7231	0.2010	0.0488	bCH(61), bCH(35)
998ms	-	1069	1039	1.4715	7.6208	0.7001	1023	1007	1.9245	4.8174	0.7472	bCH(68), CH3ipr(29)
976vs	-	1054	1023	1.0267	3.3566	1.6017	998	987	0.6272	0.3401	0.2340	bCH(67), CH3ipr(30)
916vs	-	1023	1001	5.1768	31.5553	7.9995	968	924	4.1843	29.261	7.0928	CH3ipr(66), bCN(32)
-	883vw	903	896	1.6557	23.8658	0.4911	914	887	1.5333	18.2664	0.4762	CH3ipr(65), NO2sciss(30)
869ms	-	887	866	0.8183	35.0342	0.9669	901	873	0.5880	35.442	0.4791	bCN(62), NO2wag(31)
851vs	-	872	861	1.7372	14.7314	3.6330	988	855	2.1935	7.8292	9.1458	NO2sciss(61), ωCH(22)
840ms	-	860	851	2.1050	18.5362	4.8287	973	844	1.3043	11.5592	0.2433	NO2wag(60), ωCH(27)
776ms	-	830	835	1.1987	13.6487	5.3267	934	778	1.2111	15.9929	6.3851	ωCH(51), bCC(35)
-	752vw	812	809	0.9921	0.8069	1.0931	915	756	0.9718	2.2649	2.5479	ωCH(58), bCO(32)
745vs	-	805	800	1.1038	8.6232	13.5470	889	749	0.7108	0.5416	1.5742	ωCH(57), bCO(39)
739w	-	790	785	1.0700	1.7676	4.7339	830	743	0.8465	0.2442	7.6360	NO2rock(56), ωCH(38)
728w	-	777	771	0.6233	6.9910	1.5021	781	732	0.6188	1.1593	5.0525	bCC(44), tRasym(32)
-	680vw	768	755	0.6397	6.4354	1.0886	719	684	0.4853	1.6928	0.4246	bCO(51), tRsymd(38)
640vw	-	745	735	0.5584	2.8908	3.1299	677	644	0.4957	0.1962	3.6634	bCO(50), tRtrigd(49)
622vw	622w	723	712	0.2757	0.7238	1.9933	635	624	0.2361	1.8036	4.4869	t Rasym(44), ωCC(41)
598w	-	708	698	0.2687	2.2776	0.3882	660	599	0.0817	0.9717	0.4309	t Rsymd(45), ωCO(40)
-	569w	690	678	0.1066	1.0396	2.1909	631	573	0.1092	4.9423	0.0705	t Rtrigd(50), ωCN(46)
-	554w	678	663	0.1519	3.4704	0.3266	607	559	0.1075	0.3251	2.4707	ωCC(40)
-	524w	654	645	0.0834	0.8627	3.7644	601	527	0.0348	0.1472	1.9280	ωCO(45)
-	479vw	634	623	0.0146	0.4515	0.1832	563	483	0.0972	2.0378	1.4083	ωCO(47)
-	385vw	623	612	0.0160	1.3762	0.2214	525	389	0.0099	0.3523	0.1913	ωCN(46)
-	342vs	455	412	0.0230	5.1544	0.3923	503	347	0.0328	0.0900	2.0186	NO2twist(49)
-	215s	427	412	0.0153	4.5374	1.3341	444	218	0.0101	5.2598	0.7334	tCH3(47)
-	176ms	408	399	0.0329	0.0709	3.2964	420	179	0.0157	0.5548	4.1768	tCH3(43)

Abbreviations: ν - stretching; b - in-plane bending; ω - out-of-plane bending; asymd - asymmetric; symd - symmetric; t - torsion; trig - trigonal; w - weak; vw - very week; vs - very strong; s - strong; ms - medium strong; ss - symmetric stretching; ass - asymmetric stretching; ips - in-plane stretchingj; ops - out-of-plane stretching; sb - symmetric bending; ipr - in-plane rocking; opr - out-of-plane rocking; opb - out-of-plane bending.

Table 5. The thermodynamic parameters of 3-methyl-2-nitroanisole calculated at HF/6-311++G(d,p) with and B3LYP/6-311++G(d,p) and 6-311++G(d,p) method and basis set calculations.

Parameters	HF/ 6-311++G(d,p)	B3LYP/ 6-311++G(d,p)
Optimized global minimum Energy, (Hartrees)	-587.1106	-590.7489
Total energy(thermal), E_{total} (kcal mol^{-1})	116.454	108.908
Translational	0.889	0.889
Rotational	0.889	0.889
Vibrational	28.965	107.130
Molar capacity at constant volume, (cal mol^{-1} k^{-1})		
Total	38.377	41.220
Translational	2.981	2.981
Rotational	2.981	2.981
Vibrational	34.124	35.259
Entropy		
Total	102.089	105.246
Translational	41.248	41.258
Rotational	30.397	30.519
Vibrational	29.897	33.479
Zero point vibrational energy, (Kcal mol^{-1})	109.7325	101.7850
Rotational constants (GHZ)		
A	1.1839	1.1822
B	1.0719	0.9992
C	0.6168	0.5857
Rotational temperature (Kelvin)	0.0568 0.0514 0.0296	0.0567 0.0479 0.0281

where E_0 is the energy of the unperturbed molecules, F_α the field at the origin and μ_α, $\alpha_{\alpha\beta}$ and $\beta_\alpha\beta_\gamma$ are the components of dipole moment, polarizability and the first hyperpolarizabilities, respectively. The total static dipole moment μ, the mean polarizability α_0 and the mean first hyperpolarizability β_0, using the *x*, *y*, *z* components they are defined as:

$$\alpha_0 = \frac{\left(\alpha_{xx} + \alpha_{yy} + \alpha_{zz}\right)}{3}$$

$$\alpha = 2^{-1/2}\left[\left(\alpha_{xx} - \alpha_{yy}\right)^2 + \left(\alpha_{yy} - \alpha_{zz}\right)^2 + \left(\alpha_{zz} - \alpha_{xx}\right)^2 + 6\alpha_{xx}^{\ 2}\right]^{1/2}$$

$$\beta_0 = \left(\beta_x^2 + \beta_y^2 + \beta_z^2\right)^{1/2}$$

$$\beta_{vec} = \frac{3}{5\left[\left(\beta_x^2 + \beta_y^2 + \beta_z^2\right)^{1/2}\right]}$$

where

$$\beta_x = \beta_{xxx} + \beta_{xyy} + \beta_{xzz}$$

$$\beta_y = \beta_{yyy} + \beta_{yxx} + \beta_{yzz}$$

$$\beta_z = \beta_{zzz} + \beta_{zxx} + \beta_{zyy}$$

The β_0 components of GAUSSIAN 09W output are reported in atomic units and therefore the calculated values are converted into e.s.u. units (1 a.u. = 8.3693 × 10^{-33} e.s.u.). The calculated value of hyperpolarizability and polarizability of MNA are tabulated in Table 6, respectively.

The title molecules are an attractive object for future studies of non-linear optical properties.

Table 6. Nonlinear optical properties of 3,4-dimethylanisole and 3-methyl-2-nitroanisole calculated at HF/6-311++G(d,p) with B3LYP/6-311+G(d,p) and 6-311++G(d,p) method and basis set calculations.

NLO behaviour	MNA	
	HF/ 6-311+G(d,p)	B3LYP/ 6-311++G(d,p)
Dipole moment(μ)	0.9606Debye	1.2182Debye
Mean polarizability (α)	0.8846 × 10^{-30} esu	0.9909 × 10^{-30} esu
Anisotropy of the polarizabilty (Δ_α)	1.7675 × 10^{-30} esu	1.2708 × 10^{-30} esu
First hyperpolarizability (β)	1.6177 × 10^{-30} esu	2.9059 × 10^{-30} esu
Vector – first hyperpolarizability (β_{vec})	0.9706 × 10^{-30} esu	1.7435 × 10^{-30} esu

7. HOMO-LUMO Band Gap

This electronic absorption corresponds to the transition from the ground to the first excited state and is mainly described by one electron excitation from the highest occupied molecular orbital (HOMO) to the lowest unoccupied molecular orbital (LUMO)[24]. Many organic molecules, containing conjugated π electrons are characterized by large values of molecular first hyper polarizabilities and analyzed by means of vibrational spectroscopy. In most of the cases, even in the absence of inversion symmetry, the band in the Raman spectrum is weak in the IR spectrum and vice-versa. But the intra molecular charge from the donor to acceptor group through a single-double bond conjugated path can induce large variations of both the molecular dipole moment and the molecular polarizability, making IR and Raman activity strong at the same time. The analysis of the wave function indicates that the electron absorption corresponds to the transition from the ground to the first excited state and is mainly described by one-electron excitation from the highest occupied molecular orbital (HOMO) to the lowest unoccupied orbital (LUMO). In MNA, the HOMO is located over heterocyclic ring and the HOMO-LUMO transition implies an electron density transfer to the CH_3, NO_2 group from heterocyclic ring and oxygen atom, whereas in MNA the HOMO is located over benzene ring, especially on nitro and oxygen atom, and the HOMO-LUMO transition implies an electron density transfer to the heterocyclic ring from nitro group and oxygen atom. Moreover, the composition of HOMO and LUMO for MNA is shown in Fig. 5, respectively. The HOMO-LUMO energy gap of MNA are calculated at B3LYP/6-311++G(d,p) level, which reveals that the energy gap reflects the chemical activity of the molecules. The LUMO as an electron acceptor (EA) represents the ability to obtain an electron (ED) and HOMO represents ability to donate an electron (ED).The ED groups to the efficient EA groups through π -conjugated path. The strong charge transfer interaction through π-conjugated bridge results in substantial ground state Donor-Acceptor (DA) mixing and the appearance of a charge transfer band in the electron absorption spectrum. The HOMO and LUMO energy gap explains the fact that

eventual charge transfer interaction is taking place within the title molecules.

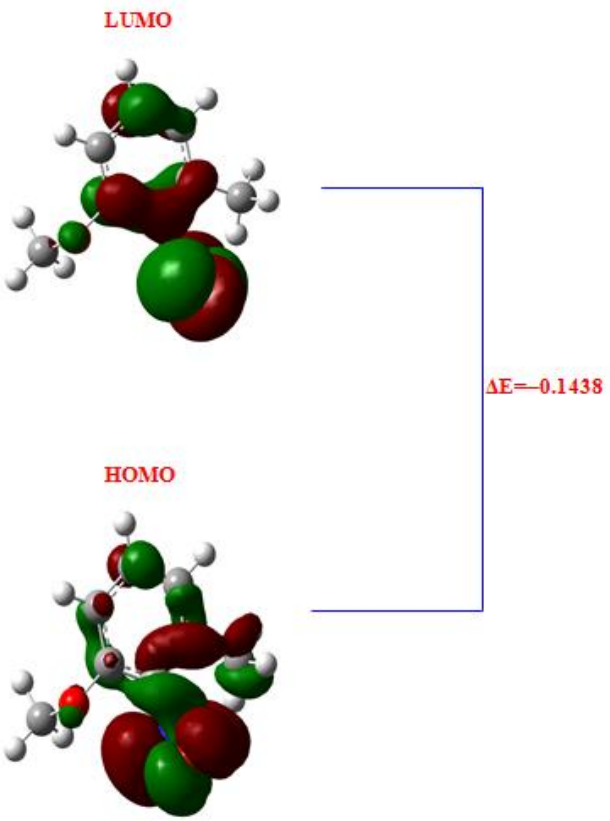

Fig 5. HOMO-LUMO plot of 3-methyl-2-nitro anisole.

7.1. Global and local reactivity descriptors

Based on density functional descriptors global chemical reactivity descriptors of compounds such as hardness, chemical potential, softness, electronegativity and electrophilicity index as well as local reactivity have been defined [25]. Pauling introduced the concept of electronegativity as the power of an atom in a compound to attract electrons to it. Hardness (η), chemical potential (μ) and electronegativity (χ) and softness are defined follows.

$$\eta = \frac{1}{2}\left(\partial^2 E/\partial N^2\right)_{V(r)} = \frac{1}{2}\left(\partial\mu/\partial N\right)_{V(r)}$$

$$\mu = \left(\partial E/\partial N\right)_{V(r)}$$

$$\chi = -\mu = -\left(\partial E/\partial N\right)_{V(r)}$$

where E and $V(r)$ are electronic energy and external potential of an N-electron system respectively. Softness is a property of compound that measures the extent of chemical reactivity. It is the reciprocal of hardness.

$$S = \frac{1}{\eta}$$

Using Koopman's theorem for closed-shell compounds, η, μ and χ can be defined as

$$\eta = \frac{(I - A)}{2}$$

$$\mu = \frac{-(I + A)}{2}$$

$$\chi = \frac{(I + A)}{2}$$

where A and I are the ionization potential and electron affinity of the compounds respectively. Electron affinity refers to the capability of a ligand to accept precisely one electron from a donor. However in many kinds of bonding viz. covalent hydrogen bonding, partial charge transfer takes places. Recently Parr *et al.* [26] have defined a new descriptor to quantity the global electrophilic power of the compound as electrophilicity index (ω), which defines a quantitative classification of the global electrophilic nature of a compound have proposed electrophilicity index (ω) as a measure of energy lowering due to maximal electron flow between donor and acceptor. They defined electrophilicity index (ω) as follows.

$$\omega = \mu^2/2\eta$$

The usefulness of this new reactivity quantity has been recently demonstrated in understanding the toxicity of various pollutants in terms of their reactivity and site selectivity. The calculated value of electrophilicity index describes the biological activity for MNA respectively. All the calculated values of HOMO-LUMO, energy gap, ionization potential, Electron affinity, hardness, potential, softness and electrophilicity index are shown in Table 7, respectively.

8. Nbo Analysis

NBO analysis gives information about interactions in both filled and virtual orbital spaces that could enhances the analysis of intra- and intermolecular interactions. The larger the $E^{(2)}$ (energy of hyperconjugative interactions) value, the more intensive is the interaction between electron donors and electron acceptors, i.e. the more donating tendency from electron donors to electron acceptors the greater the extent of conjugation of the whole system. Delocalization of electron density between occupied Lewis-type (bond or lone pair) NBO orbitals and formally unoccupied (anti-bond or Rydberg) non-Lewis NBO orbitals correspond to a stabilizing donor–acceptor interaction. NBO analysis has been performed on the title molecule at the DFT level in order to elucidate the intra-molecular, re-hybridization and delocalization of electron density within the molecule. The larger $E^{(2)}$ value, the more intensive is the interaction between electron donors and acceptors, i.e., the more donation tendency from electron donors to electron acceptors and the greater the extent of conjugation of the whole system. DFT (B3LYP/6-311++G(d,p)) level computation is used to investigate the various second-order interactions between the filled orbitals of one subsystem and vacant orbitals of another subsystem, which is a measure of the delocalization or hyper-conjugation [27]. NBOs are localized electron pair orbitals for bonding pairs and lone pairs. The hybridization of the atoms and the weight of each atom in each localized electron pair bond are calculated in the idealized Lewis structure. A normal Lewis structure would not leave any antibonding orbitals, so the presence of antibonding orbitals shows deviations from normal Lewis structures. Anti bonding localized orbitals are called non-Lewis NBOs. In order to study the small deviations from idealized Lewis structure, the Donor–Acceptor interaction approach is adopted. In MNA, π(C3–C4)→π*(C1–C2), π(C5–C6)→ π*(C1–C2) interaction is seen to give a strong stabilization 41.84 and 52.46 kJ/mol. This strong stabilization denotes the larger delocalization. The interesting interactions in MNA molecule are LP1N12, LP2O7with that of antibonding O13–O14, C1–C6. These two interactions result the stabilization energy of 162.54, 13.84 kJ/mol respectively. This highest interaction around the ring can induce the large bioactivity in the molecule. This shows that the lone pair orbital

participates in electron donation in the molecule. The calculated values of $E^{(2)}$ are shown in Table 8 for MNA, respectively.

9. ^{13}C AND ^{1}H NMR SPECTRAL ANALYSIS

The molecular structure of MNA is optimized by using B3LYP method with 6-31++G basis set. Then, GIAO ^{13}C calculations of the title compound are calculated and compared with experimental values [28] are shown in Table 9. Relative chemical shifts are then estimated by using the corresponding TMS shielding calculated in advance at the theoretical level as reference. Changes in energy needed to flip protons are called chemical shifts. The location of chemical shifts (peaks) on a NMR spectrum are measured from a reference point that the hydrogen in a standard reference compound –$(CH_3)_4Si$ or tetramethylsilane (TMS)– produce. The amount of energy necessary to flip protons in TMS is assigned the arbitrary value of zero δ. Chemical shifts are measured in parts per million magnetic field strength difference (δ-scale), relative to TMS. The experimental values of MNA for ^{1}H and ^{13}C isotropic chemical shielding for TMS are 161.30, 163.80 ppm, respectively [28]. All the calculations are performed using Gauss view molecular visualization program and Gaussian 09W program package. The result shows that the range ^{13}C NMR chemical shift of the typical organic compound usually is > 100 ppm, the accuracy ensures reliable interpretation of spectroscopic parameters. It is true from the above literature value in our present study, that the title compound also shows the same. In practice, it is easier to fix the radio wave frequency and vary the applied magnetic field than it is to vary the radio wave frequency. The magnetic field "felt" by a hydrogen atom is composed of both applied and induced fields. The induced field is a field created by the electrons in the bond to the hydrogen and the electrons in nearby π bonds. When the two fields reinforce each other, a smaller applied field is required to flip the proton. In this situation, a proton is said to be deshielded. When the applied and induced fields oppose each other, a stronger field must be applied to flip the proton. In this state, the proton is shielded. Electronegative atoms such as CH_3, O, NO_2 and halogens deshield hydrogen. The extent of deshielding is proportional to the electronegativity of the heteroatom and its proximity to the hydrogen. These nitro and oxygen atoms show electronegative property, so that the chemical shift of C1, C2, C3, C4, C5, C6 for MNA seems to be 161.28, 163.80, 141.74, 121.87, 131.91 and 122.65 ppm. The chemical shift of C9 is greater than the other carbon values. This increase in chemical shift is due to the substitution of more electronegative oxygen and nitro atoms in the benzene ring. The presence of electronegative atom attracts all electron clouds of carbon atoms towards the oxygen and nitro atoms, which leads to deshielding of carbon atom and net result in increase in chemical shift value. The NMR shielding surfaces of C15, C8 is shown in this work the chemical shift (δ) for carbon atoms presented in the MNA in gas phase has been studied and theoretical ^{13}C, ^{1}H-NMR isotropic shielding of carbon and Hydrogen atom. In the NMR shielding surfaces, the blue region represents shielding and red region represents de-shielding are shown in Fig. 6 for MNA, respectively.delocalization of electron density within the molecule.

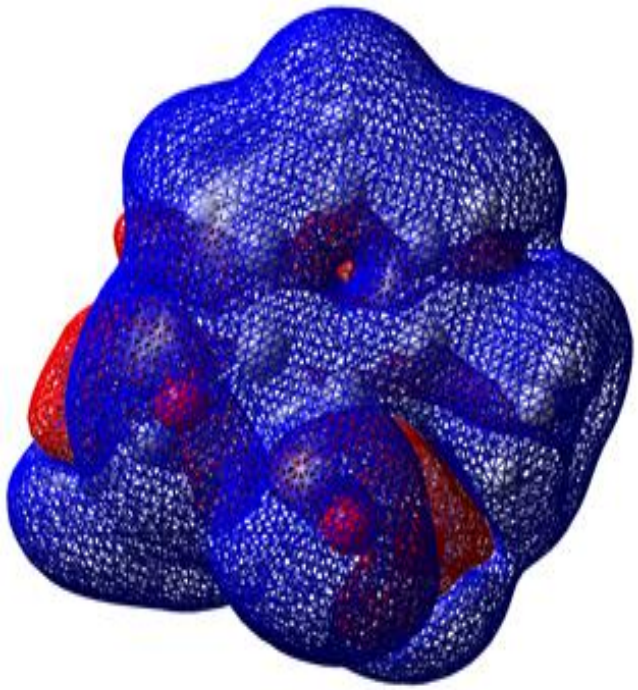

Fig 6. NMR shielding surface of 3-methyl-2-nitro anisole.

10. Conclusion

The molecular structural parameters, thermodynamic properties and fundamental vibrational frequencies of the optimized geometry of 3-methyl-2-nitroanisole have been obtained from *ab initio* HF and DFT calculations. The theoretical results are compared with the experimental vibrations. The computed geometrical parameters are in good agreement with the observed X-ray diffraction data of similar compound. Although both types of calculations are useful to explain vibrational spectra of 3-methyl-2-nitroanisole, *ab initio* calculations at HF/6-311++G(d,p) level is found little poorer than DFT-B3LYP/6-311++G(d,p) level calculations. On the basis of agreement between the calculated and experimental results, assignments of all the fundamental vibrational modes of 3-methyl-2-nitroanisole have been made for the first time in this investigation. The TED calculation regarding the normal modes of vibration provides a strong support for the frequency assignment. Therefore, the assignments proposed at higher level of theory with higher basis set with only reasonable deviations from the experimental values seem to be correct. HOMO and LUMO energy gap explains the eventual charge transfer interactions taking place within the molecule. Furthermore, the nonlinear optical, first-order hyperpolarizabilities and total dipole moment properties of the molecule show that the title molecule is an attractive object for future studies of nonlinear optical properties. NMR, NBO analysis have been performed in order to elucidate charge transfers or conjugative interaction, the intra-molecule rehybridization and delocalization of electron density within the molecule.

Reference

[1] Hiers G.S, Hager F.D, Org. Synth. Collect. 1 (1941) 58–60.
[2] Rumi M, Zerbi G, J. Mol. Struct. 509 (1999) 111–115
[3] Gordon JP, Leite RCC, Moore RS, Porte SPS, Whinnery JR, Journal of Applied Physics, 36 (1965) 3.
[4] Sheldon SJ, Knight LV, Thorne JM, Applied Optics, 21 (1982) 1663.
[5] Jurgensen F, Schroer W, Applied Optics, 34 (1995) 41.

[6] Frisch MJ, Trucks GW, Schlegal HB, GAUSSIAN 09, Revision A.02, Gaussian, Inc., Wallingford, CT, 2009.
[7] Schlegel HB, Comput J. Chem. 3 (1982) 214.
[8] Becke AD, Chem J. Phys. 98 (1993) 5648.
[9] Lee C, Yang W,. Parr R G, Phys. Rev. B37 (1988) 785.
[10] Pulay P, Fogarasi G, Pongor G,. Boggs JE, Vargha A, Am. Chem J. Soc. 105 (1983) 7037.
[11] Rauhut G, Pulay P, Phys J. Chem. 99 (1995) 3093.
[12] Fogarasi G, Ulay P, in: Durig JR (Ed.) Vibrational Spectra and Structure, Vol.14, Elsevier, Amsterdam, 1985, P. 125, Chapter 3.
[13] Fogarasi G, Zhou X, Taylor PW, Pulay P, J. Am. Chem. Soc. 114 (1992) 8191-8201.
[14] Sundius T, J. Mol. Struct., 218 (1990) 321.
[15] Sundius T, Vib. Spectrosc., 29 (2002) 89.
[16] MOLVIB (V.7.0): Calculation of Harmonic Force Fields and Vibrational Modes of Molecules, QCPE Program No. 807 (2002).
[17] Frisch A, Nielson AB, Holder AJ, Gaussview User Manual, Gaussian Inc., Pittsburg, PA, 2000.
[18] Polavarapu PL, J. Phys. Chem. 94 (1990) 8106.
[19] Keresztury G, Raman spectroscopy theory, in: JM Chalmers, P, Griffiths R (Eds.), Handbook of Vibrational Spectroscopy, Vol. 1, John Wiley & Sons Ltd., 2002, p. 71.
[20] Keresztury G, Holly S, Varga J, Besenyei G, Wang AY, Durig JR, Spectroschim Acta part 49A (1993) 2007.
[21] Qu Y, Sun XM, Acta Crystallography, E 61 (2005) 3828.
[22] Sambathkumar K, Density Functional Theory Studies of Vibrational Spectra, Homo- Lumo, Nbo and Nlo Analysis of Some Cyclic and Heterocyclic Compounds (Ph.D. thesis), Bharathidasan University, Tiruchirappalli, August 2014.
[23] Kuppusamy Sambathkumar Spectrochim. Acta A 147 (2015) 51-66.
[24] Sambathkumar K, *Elixir Vib.Spec. 91 (2016) 38381-38391*.
[25] Parr RG, Szentpaly LV, Liu SJ, Am. Chem. Soc., 121 (1999) 1922.
[26] Sambathkumar K, Jeyavijayan S , Arivazhagan M Spectrochim. Acta A 147 (2015)51-66.
[27] Sambathkumar K, Claude A and Settu K Elixir Vib. Spec.91 (2016) 38368-38380.
[28] http://riodbol.ibase.aist.go.jp/sdbs/(National Institute of Advanced Industrial Science).